Solubility and Structure of Calcium Silicate Hydrate

Jeffrey J. Chen[†]*, Jeffrey J. Thomas[‡], Hal F.W. Taylor[§], and Hamlin M. Jennings[†‡]*

Northwestern University, Department of Materials Science and Engineering, Evanston, IL 60208;

Northwestern University, Department of Civil and Environmental Engineering, Evanston, IL 60208;

Maundry Bank, Lake Road, Coniston, Cumbria, LA21 8EW, UK

*Corresponding authors: jjchen@alumni.princeton.edu, h-jennings@northwestern.edu

† Northwestern University, Department of Materials Science and Engineering

‡ Northwestern University, Department of Civil and Environmental Engineering

§ Deceased as of November 25, 2002

Abstract. A poorly crystalline class of calcium silicate hydrates known as C–S–H possesses extensive disorder and structural variations at the nanometer scale. The extent of these variations has generally obscured a comprehensive understanding of the C–S–H nanostructure, but new relationships between solubility and structure appear to shed new light on this old problem. These relationships were inspired from the discovery in the $CaO–SiO_2–H_2O$ system at room temperature of a family of new C–S–H solubility curves: A, C'', C', and C (Figure 9). ^{29}Si magic-angle spinning (MAS) NMR studies and charge balance calculations suggest that these variations in solubility reflect systematic variations in structure of which those in Ca/Si ratio, silicate polymerization, and Ca–OH content appear most important. These findings define more explicit relationships between the nanostructure of C–S–H and the crystal structures of 1.4-nm tobermorite and jennite. C–S–H that equilibrates with aqueous solution

on curve A, for example, is believed to have a purely tobermorite-like structure (i.e. one with no Ca–OH), which at saturation in $Ca(OH)_2$ has a Ca/Si ratio of 1.5 and a silicate anion structure fragmented to the minimum possible mean chain length of 2. C–S–H samples that equilibrate on curves C", C', and C have progressively higher Ca/Si ratios at saturation in $Ca(OH)_2$ and, for a given Ca/Si ratio, higher mean chain lengths and Ca–OH contents. Given these trends, curves A, C", C', and C are solubility curves for a spectrum of C–S–H structures formed at room temperature, ranging from a purely tobermorite-like structure on curve A to a largely jennite-like configuration on C.

1 Introduction

Calcium silicate hydrates possess a remarkable level of structural complexity. Over 30 crystalline phases are known, and for preparations near room temperature, there is an indefinite range of semi-crystalline to nearly amorphous phases, all of which are described by the generic term, C–S–H. The structure of C–S–H, particularly that produced from the reaction of portland cement and water, has been studied extensively, and while certain details are still uncertain, there is good evidence[1] that the structure at the nanometer or "crystal-chemical" level most closely resembles imperfect forms of the minerals, 1.4-nm tobermorite[2], $Ca_5Si_6O_{16}(OH)_2 \bullet 8H_2O$, and jennite[3], $Ca_9(Si_6O_{18})(OH)_6 \bullet 8H_2O$. Both have layered structures that are reminiscent of those in clay minerals[4]. In fact, it has been shown[5] that substituted forms of C–S–H show selective cation exchange for some hazardous metals, thus emulating the behavior of certain clay minerals and zeolites. More recently, it has been demonstrated[6] that organic polymers can intercalate into the structure of C–S–H, thereby suggesting promising synthetic routes for novel organic-inorganic nanocomposite materials[7] with potentially useful and interesting properties.

The success of many applications involving chemical interactions with C–S–H depends largely on knowledge of the structure at the nanometer scale. A comprehensive understanding at this level, however, is somewhat obscured by the extensive variations in C–S–H: the Ca/Si ratio, degree of crystallinity, and degree of silicate polymerization can all vary widely, and to some extent, independently. A full understanding of the structure of C–S–H is therefore one that can most completely

describe how the structure varies, and how these variations are related.

New phase equilibrium and ^{29}Si magic-angle (MAS) NMR studies on C–S–H show that variations in solubility are intimately related to those in structure. From these findings, we describe a family of C–S–H structures that form at room temperature, and discuss simple ways by which variations occur. While these relationships have immediate bearing on the chemistry of C–S–H and cements, the approach used here may also have general applicability to the study of disorder in other silicate phases.

1.1 Relationship of C–S–H to more crystalline phases. Much of our knowledge of the short-range order in C–S–H has been obtained from structural comparisons with crystalline calcium silicate hydrates, 1.4-nm tobermorite and jennite being the most appropriate models.

The structure of 1.4-nm tobermorite, $Ca_5Si_6O_{16}(OH)_2 \bullet 8H_2O$, which has only recently been properly solved[2], has long been known to be based on a composite layer composed of a distorted central Ca–O sheet that is ribbed on either side with infinite dreierketten, i.e. silicate chains that repeat at an interval of every three silicate tetrahedra (Figure 1). Two of these, called paired tetrahedra, share two oxygen atoms with the central Ca–O sheet, while the third, called a bridging tetrahedron, shares only one. The particular conformation of a dreierkette reflects the need for the silicate chain to conform to the interatomic spacings of the Ca–O sheet, which itself is dictated by the coordination requirements of the Ca cation. The interlayer spaces contain water molecules and additional Ca cations, which balance the negative charge of the composite layer. The Ca/Si ratio of an idealized structure of 1.4-nm tobermorite is 0.83, but as will be discussed, this value can easily increase in less ordered forms.

The crystal structure of jennite, $Ca_9(Si_6O_{18})(OH)_6 \bullet 8H_2O$, has only recently been determined[3], though the Ca–O part and some other features were suggested on crystal chemical grounds in an otherwise imperfect model of the structure in 1968[8]. Like that of 1.4-nm tobermorite, it is based on layers in which a central Ca–O sheet is flanked on both sides by rows of dreierketten, together with interlayer Ca atoms and water molecules. However, there are major differences, and statements in the literature that jennite has a tobermorite-type structure in which alternate silicate chains are replaced by OH groups are

misleading. The Ca–O layers in jennite have the empirical formula Ca_2O_5 and are highly corrugated; some of their O atoms are shared with the dreierketten, the paired tetrahedra of which are inset within the corrugations, while others form parts of OH groups, thereby forming Ca–OH bonds. The constitutional formula is probably $Ca_9(Si_6O_{18})(OH)_6{\cdot}8H_2O$, though synthetic preparations seem always deficient in interlayer Ca, charge balance being maintained by the presence of Si–OH groups. The Ca/Si ratio of jennite, of or slightly below 1.5, is considerably higher than that of 1.4-nm tobermorite.

1.2 C–S–H(I), C–S–H(II), and C–S–H gel. An important characteristic of the tobermorite structure is its ability to vary in composition, degree of polymerization, and extent of crystallinity without destroying the essential features of the composite layer structure. A related phase known as C–S–H(I)[9], which is formed by reaction of hydrous silica with lime in aqueous suspension at room temperatures, or by mixing an alkali silicate with a calcium salt under similar conditions (a reaction known as double decomposition), is a very imperfect version of 1.4-nm tobermorite. X-ray diffraction (XRD) powder patterns consist largely of *hk*0 bands of 1.4-nm tobermorite and, under certain conditions, a broad basal reflection, all of which suggests a material having little more than two-dimensional order. C–S–H(I) can accommodate a substantial concentration of defects such as the omission of bridging tetrahedra[4], or variations in the contents of interlayer Ca and of H attached to Si–O. Removal of bridging tetrahedra fragments the infinite silicate chains into finite segments (Figure 1), thereby causing the mean chain length, which can be deduced from ^{29}Si MAS NMR, to decrease with increasing Ca/Si ratio[10,11].

The phase C–S–H(II), which is produced from a somewhat uncertain[12] prolonged reaction of tricalcium silicate (Ca_3SiO_5) or β-dicalcium silicate (Ca_2SiO_4) with excess water, is probably an imperfect version of jennite, to which it appears to be related somewhat as C–S–H(I) is to 1.4-nm tobermorite. The preparations that have been described have had Ca/Si ratios slightly under 2.

Ca_3SiO_5 or Ca_2SiO_4 are the main constituents of portland cement, and the reaction of these compounds with about half their weight of water produces a hardened paste containing two products, C–S–H gel and calcium hydroxide, $Ca(OH)_2$. C–S–H gel is even less ordered than C–S–H(I) or C–S–H(II),

its XRD powder pattern consisting of a broad band at 0.26–0.32 nm and a sharper one at 0.182 nm. Spacings in these regions are shown by both 1.4-nm tobermorite and jennite and it has not been possible to conclude from XRD evidence which structure better approximates the short-range order in C–S–H gel. Determinations of the contents of $Ca(OH)_2$ and residual Ca_3SiO_5, and microanalyses using the microprobe or scanning electron microscope (SEM) indicate a Ca/Si ratio in C-S-H gel of 1.7–1.8. These observations, combined with other evidence from transmission electron microscope (TEM) microanalysis, density, silicate polymerization, and water content, have led to the hypothesis that, at late ages, the C–S–H produced from Ca_3SiO_5 resembles an imperfect form of jennite more closely than an imperfect form of 1.4-nm tobermorite[13].

1.3 Previous relations in the phase equilibria of the $CaO–SiO_2–H_2O$ system. Except at low Ca/Si ratios, C–S–H will dissolve incongruently in water or solutions of $Ca(OH)_2$, the Ca/Si ratio of C–S–H thus changing accordingly until equilibrium is reached. Numerous investigations have studied this apparently simple phenomenon, and despite the progress in understanding the structure of C–S–H, comprehension of the variations in phase equilibria of the $CaO–SiO_2–H_2O$ system at room temperature has proven very challenging. Early studies generated a particularly disconcerting variety of results, making interpretations rather speculative in many areas (see review by Steinour[14]).

In a later analysis of the data, Jennings[15] plotted numerous published solubility data as Ca versus Si concentration and showed evidence for two well-defined solubility curves of differing Si concentrations (see Figure 2). The curve lower in Si concentrations, curve A, was considered to be the solubility curve for C–S–H(I). This conclusion was reached from XRD powder evidence, and the fact that most of the points on the curve were obtained from preparations of lime and hydrous silica in suspension or by the double decomposition of sodium silicate with a calcium salt. The curve with higher Si concentrations, curve B, was obtained solely from experiments measuring concentrations during the first several hours after initial contact of Ca_3SiO_5 with water; since C–S–H has not yet formed to an appreciable extent during this time, it was presumed that curve B represented a metastable solubility curve for the initial

product formed as a layer on the Ca_3SiO_5 surface. Barret and Bertrandie[16] later disputed this conclusion and claimed that curve B was not a true solubility curve, but instead resulted from a transitory kinetic balance between the dissolution of a hydroxylated surface layer on Ca_3SiO_5 and the precipitation of C–S–H. While the two views have different interpretations, both assume the presence of an altered surface layer on Ca_3SiO_5 that is metastable with respect to C–S–H.

1.4 Weaknesses in previous phase equilibrium relations. While the establishment of two distinct solubility curves in the $CaO–SiO_2–H_2O$ system was a significant advance, several important questions remained unanswered. There are, for example, surprisingly few studies reporting the solubility of mature C–S–H gel produced from Ca_3SiO_5 paste, which as mentioned above, is known to be considerably less ordered and of higher Ca/Si ratio than C–S–H(I). Despite these differences, it has generally been presumed, on the basis of indirect evidence from dilute Ca_3SiO_5 suspensions, that a fully hydrated Ca_3SiO_5 paste will eventually equilibrate to the solubility curve of C–S–H(I) (i.e. curve A). The data from the only known study[17] to report Ca and Si concentrations for mature Ca_3SiO_5 pastes, however, do not show agreement with either curve A or B and, in fact, points appear erratically scattered between the two curves where it was originally presumed[15] that few data points (with the exception of ones obtained from hydrated β-Ca_2SiO_4) could exist.

The maximum Ca/Si ratio in C–S–H occurs when it is in equilibrium in aqueous solution with solid $Ca(OH)_2$. These values, however, can vary considerably, and those cited range from as low as 1.3 to as high as 2, those between 1.5 and 1.7–1.8 having been generally considered the most probably correct. The cause of this variability does not appear to be solely linked to starting solid materials, and other than experimental error or possible non-equilibrium conditions[14], no explanation has been proposed.

There are no reported solubility data on jennite or C–S–H(II), and little is known of the phase equilibria relating to a jennite-type C–S–H. One could speculate that the scatter on curve A at high Ca concentrations is due to jennite-like conformations, but without supporting evidence this suggestion cannot be made with confidence. It should also be mentioned that curve B does not represent the

solubility curve for C–S–H(II) or, more generally, jennite-like C–S–H as is sometimes mistakenly assumed. This interpretation was offered speculatively in the original discussion of the plot of Ca versus Si concentration[15], but the conjecture was not well substantiated.

1.5 Current investigation. Given the uncertainties in the phase equilibrium relations noted above, it appeared worthwhile to carefully analyze and contrast C–S–H preparations of two distinctly different types. One was obtained from a relatively well-hydrated Ca_3SiO_5 paste, the other from a preparation made by double decomposition of $Ca(NO_3)_2$ and Na_2SiO_3. Phase equilibrium determinations show evidence for a family of new solubility curves at high Ca concentrations. ^{29}Si MAS NMR studies on solids collected from these experiments point to logical routes by which variations in C–S–H at high Ca/Si ratios occur. This development has made it possible to more fully address some of the uncertainties on such issues as the variations in Ca/Si ratio at $Ca(OH)_2$ saturation, and the structural relationships between tobermorite and jennite-like forms of C–S–H.

2 Experimental

2.1 Preparative methods. *Tricalcium silicate pastes*. Ca_3SiO_5 was prepared by firing 3:1 molar mixtures of reagent grade lime and fumed silica at temperatures slightly exceeding 1450ºC. As determined by XRD, three firings were necessary for complete reaction, and prior to each, samples were quickly cooled to room temperature, ground into a powder, and then pressed into discs to enhance uniformity of the product.

Hydrated Ca_3SiO_5 pastes were prepared with deionized water at a water-to-solids ratio of 0.50. Samples were mixed by hand and cast in cylindrical polystyrene vials measuring 25 mm in diameter and 50 mm in height. After 3 days, the hardened pastes were demolded and stored in saturated solutions of $Ca(OH)_2$ in sealed polyethylene containers. Pastes were hydrated for approximately 8 months at 22 ± 1°C. Only trace amounts of anhydrous Ca_3SiO_5 could be detected by XRD in the hydrated pastes, and the quantity of non-evaporable water retained after drying to the vapor pressure of water at 194 K (i.e. D-drying[18]) suggested that the pastes were over 95% hydrated. Solids derived from the Ca_3SiO_5 pastes

will be described as belonging to the Ca_3SiO_5 group.

Double decomposition of calcium nitrate with sodium silicate. A 0.050-mole quantity of reagent grade $Na_2SiO_3 \bullet 5H_2O$ was dissolved in 125 mL of carbon dioxide free deionized water to which was added 0.075 moles of reagent grade $Ca(NO_3) \bullet 4H_2O$ that was dissolved in 75 mL of carbon dioxide free deionized water. Stirring was continued for one hour in a tightly sealed plastic container filled with nitrogen gas. The C–S–H precipitate was then washed with 2 L of a 20 mM $Ca(OH)_2$ solution on a Buchner funnel under a continuous stream of nitrogen. After the wash solution had passed through the solid, the sample was flushed with nitrogen and tightly sealed in a plastic container. The C–S–H precipitate had a Ca/Si ratio of 1.40 with only trace amounts of residual alkali detectable by inductively coupled plasma atomic emission spectroscopy (ICP-AES). Solids derived from the preparation made by double decomposition will be described as belonging to the double decomposition group.

Decalcification by concentrated ammonium nitrate solutions. To facilitate determinations of the solubility of C–S–H at low Ca/Si ratios, several of the samples made by both methods were decalcified in 6 M ammonium nitrate (NH_4NO_3) solutions prior to determinations of solubility (described in Section 2.2).

The leaching procedure for the Ca_3SiO_5 pastes involved immersing ~ 0.8-mm thick sample discs (cut with a diamond saw) in stirred 100-mL solutions of 6 M NH_4NO_3, thereby yielding solid-to-solution ratios of ~ 250. The weight loss of the sample, measured in the saturated surface dry state, was followed during leaching; precise correlations between weight loss and Ca/Si ratio were made. At the desired weight loss, sample discs were removed from the NH_4NO_3 solution and immediately immersed in ~ 50 mL of deionized water to remove the residual NH_4NO_3 solution residing in the pores of the paste. As supported by pore fluid exchange calculations, approximately 10–15 min of stirring in deionized water was necessary for complete replacement of the heavier NH_4NO_3 solution ($\rho \sim 1.13$ g cm^{-3}) by water.

Chemical analysis of the NH_4NO_3 leaching solutions indicated that the solids lost very little silica, even when their Ca/Si ratios decreased to well below 1, at which point the equilibrium concentration of

silica in water would have exceeded that of lime. Consequently, Ca_3SiO_5 pastes could be strictly decalcified in a very efficient manner with NH_4NO_3 solutions, removing the last traces of $Ca(OH)_2$ after ~ 40 min, and lowering the bulk Ca/Si ratio of the solid to 1.0 and 0.3 in approximately 70 min and 4 h, respectively.

A single lot of C–S–H made by double decomposition was also leached in a 6 M NH_4NO_3 solution by a procedure similar to that described above. The sample was shaken in the leaching solution for 5 min, rinsed for 10 min in deionized water, and then filtered on a Buchner funnel under a nitrogen stream. The Ca/Si ratio of the resulting solid was 0.55; XRD showed the presence of hydrous silica and C–S–H.

2.2 Phase equilibrium determinations. The analytical concentrations of Ca and Si in equilibrium with solids of the Ca_3SiO_5 and double decomposition groups were determined at 22 ± 1ºC. In all experiments a given amount of solid (ranging from 0.01–1 g) was equilibrated in 25 mL of decarbonated deionized water or $Ca(OH)_2$ solution. Samples were continuously tumbled end-over-end in 30-mL Nalgene centrifuge vials that were sealed with screw caps fitted with rubber gaskets. Equilibration times were 2–6 weeks for the samples of the Ca_3SiO_5 group, and 3 days to 2 weeks for those of the double decomposition group. The solutions were filtered under flowing nitrogen through 0.2-μm filters; the resulting filtrates were immediately acidified with HCl and then measured for Ca and Si by ICP-AES.

As outlined in Table 1, several different methods were used in the solubility experiments. These can be divided into those in which equilibrium was approached through the decalcification of a high Ca/Si solid (Series A, B, and D) and those in which it was approached through the recalcification of a low Ca/Si ratio solid (Series C, E, and F).

In most cases, determination of the Ca/Si ratio of the solid involved decomposition[19] with $LiBO_3$ at 1000ºC; the soluble glass obtained upon fusion was subsequently dissolved in dilute acid, and the resulting solution analyzed by ICP-AES. In several cases where the Ca/Si ratio was not directly determined, values were calculated from differences in the initial and final concentrations of Ca and Si

in solution; measured and calculated values of Ca/Si ratio generally agreed to within 2%.

pH values were determined on unfiltered portions of the equilibrated solution using a glass electrode.

At all stages of the solubility experiments, precautions were taken to minimize contamination by atmospheric carbon dioxide: deionized water was thus freshly boiled, samples crushed under nitrogen, and $Ca(OH)_2$ solutions prepared with freshly decomposed reagent grade $CaCO_3$.

2.3 ^{29}Si magic-angle spinning (MAS) NMR experiments. The ^{29}Si solid-state MAS NMR spectra were collected on a Varian VXR300 (7 T) spectrometer operating with a magnetic field of 59.578 MHz and a spinning rate of 4 kHz. A 5-mm zirconia rotor with Aurum caps was used for all experiments. Samples were collected for 800 scans, each scan consisting of a single pulse of width 4.7 μs followed by a delay of 10 s. Longer delay times of up to 100 s were also tried, but the improvements in the quality of the scans were considered insufficient to warrant the longer collection times. Chemical shifts are reported relative to tetramethylsilane (TMS), using tetrakis(trimethylsilyl)silane, $Si(Si(CH_3)_3)_4$, as an external standard.

Relative intensities of the Q^i ^{29}Si peaks were measured through deconvolutions of the spectra by commercial NMR spectroscopy analysis software. It is easily shown that, if C–S–H contains no Q^3, the mean chain length is given by $2(Q^1+Q^2)/Q^1$. As will be discussed, the shoulder at –83 ppm on the Q^2 peak was assigned as an integral part of the main Q^2 peak at –85 ppm.

The samples in Series L (Table 2), which were Ca_3SiO_5 pastes decalcified in NH_4NO_3 solutions, were rinsed in deionized water, lightly crushed, and then very briefly dried under nitrogen before analysis by ^{29}Si MAS NMR. Several samples from the phase equilibrium experiments of Series C in the Ca_3SiO_5 group (see Table 1) were also analyzed. Samples in the double decomposition group were selected from Series D, E, and F. The higher water contents of these samples necessitated preliminary drying for approximately 20 min under the vacuum of a rotary pump. This procedure was necessary to prevent sticking and subsequent spinning problems in the rotor.

2.4 XRD. XRD powder scans of several samples collected from the phase equilibrium experiments

were acquired with a Rigaku X-ray diffractometer with CuKα radiation operating at 40 kV and 20 mA. Scans were collected at 0.75º 2θ•min^{-1} over the range 5°–60° 2θ.

3 Results

The results of the phase equilibrium and XRD determinations are summarized in Table 2, those of the ^{29}Si MAS NMR studies in Table 3. Subsequent plots are based on these data.

3.1 Ca versus Si concentration in aqueous solution. The current investigation provides strong evidence for several new solubility curves at high Ca concentrations in the CaO–SiO_2–H_2O system at ordinary temperature. Shown in Figure 2 are the equilibrium concentrations of Ca and Si in aqueous solution for samples of the Ca_3SiO_5 and double decomposition groups; Ca/Si ratios of the solids are noted for several data points. Also plotted in this figure is curve A, the solubility curve for C-S-H(I) [15], and slightly modified versions of curve B and of the solubility curve for $Ca(OH)_2$ (see Section 4.1). The equilibrium points for both groups of preparations lie near curve A at low Ca concentrations, but depart from it at high concentrations onto two new and apparently parallel solubility curves, both of which intersect that of $Ca(OH)_2$ near 20.6 mM Ca. For the samples of the Ca_3SiO_5 group, the concentrations lie on the higher of the new curves, curve C, which departs from curve A at ~ 4 mM Ca, at which point the Ca/Si ratio of the solid is ~ 1.2. The concentrations of the double decomposition group make a similar departure from curve A onto C", but at slightly higher Ca concentration and Ca/Si values of ~ 8 mM Ca and 1.3, respectively.

As will be shown in ensuing sections, it is believed that the departures from curve A onto C or C" are caused by the introduction of Ca–OH bonds into C–S–H. This transition signifies a departure from a structure of purely tobermorite type, represented by curve A, to ones that include jennite-like characteristics in C and to a lesser extent in C".

Reversibility in phase equilibria. The validity of curves C and C" is well-supported by their reversibility; that is, there is excellent agreement between experiments that approached equilibrium through the decalcification of a high Ca/Si sample (unfilled and dotted data points in Figure 2) and those

that reached equilibrium through the recalcification of a low Ca/Si ratio sample (filled or partially filled points). This agreement is a good indication that the equilibration times allotted for the solubility experiments were sufficient. Moreover, the reversibility in solubility strongly suggests that the structural changes in C–S–H that accompany going from high to low Ca concentrations, or vice versa, are also reversible. This is supported by the reversibilities in Ca/Si ratio and mean silicate chain length illustrated below.

3.2 Ca concentration versus Ca/Si of the solid. Figure 3 is a plot of Ca concentration in aqueous solution versus the Ca/Si ratio of the solid. The vertical sections at ~ 1.2 mM Ca and 20.6 mM Ca represent conditions of three-phase equilibrium between C–S–H, solution, and either hydrous silica or $Ca(OH)_2$, respectively. The portions of the curves between ~ 1.2 to 20.6 mM Ca represent regions of two-phase equilibrium between C–S–H and aqueous solution. In general, the Ca/Si ratio increases with increasing Ca concentration.

The results in Figure 3 parallel those in solubility in that the two groups of preparations agree relatively well at low Ca concentrations, but then diverge at high values. In the two-phase region, the samples of the Ca_3SiO_5 group equilibrate on the upper curve, which leads to a relatively high Ca/Si ratio of ~ 1.8 at saturation in $Ca(OH)_2$. Those of the double decomposition group follow the lower curve, which leads to a maximum Ca/Si ratio near 1.5 at saturation in $Ca(OH)_2$. As with solubility, both groups demonstrate reversibility in the Ca/Si ratio, although with some uncertainty in the case of the samples in the Ca_3SiO_5 group as described below.

The curve in Figure 3 for the Ca_3SiO_5 group does not include samples A3–A8 because they were not believed to be in true equilibrium. The XRD data, described later, showed that all of these samples contained $Ca(OH)_2$, and, since they had been prepared by decalcification of a Ca_3SiO_5 paste, significant concentration gradients may have existed within the solid particles, so that their surface regions were in equilibrium with the solution while C–S–H of higher Ca/Si ratio and $Ca(OH)_2$ were present within them, thereby raising the Ca/Si ratio. This inhomogeneity could possibly have been eliminated or reduced by

finer grinding.

3.3 XRD. Figure 4 shows powder XRD scans for several samples from the Ca_3SiO_5 group and one sample from the double decomposition group. The results indicate a fairly low degree of order in all samples as the only relatively sharp peaks are those at 0.304, 0.279 and 0.182 nm. Since all forms of C–S–H that are sufficiently crystalline give peaks in these regions, they are of no diagnostic value. A weak peak at 0.166 nm, seen most clearly in samples B4 (Ca/Si = 0.89) and B6 (Ca/Si = 0.62) of the Ca_3SiO_5 group, is characteristic of tobermorite-type C–S–H, i.e. C–S–H(I); this is in agreement with the low Ca/Si ratios of these samples as well as their equilibration on curve A. There is no clear indication of basal reflections, except for a suggestion of one at 6º 2θ in sample B4 (Ca/Si = 0.89). Hydrous silica was only detected in the pattern of sample B7 (Ca/Si = 0.11), which shows the characteristic broad band at 22.5º 2θ. From its composition, sample B6 (Ca/Si = 0.62) might also be expected to show hydrous silica, and its absence probably indicates that little of this phase is present. The broad band between 8º and 18º 2θ could arise from the glass slide on which the sample was mounted but may include a small contribution from C–S–H(I) at 16.7° 2θ (0.53 nm).

The powder XRD scans for the samples in the double decomposition group were broadly similar to those of the Ca_3SiO_5 group. However, there are subtle differences at high Ca/Si ratios such as the sharper peaks at 0.304 and 0.279 nm, and a slightly more pronounced peak at 0.535 nm as shown in sample D3 (C/S = 1.44) of the double decomposition group. These observations could suggest greater order and a closer resemblance to a tobermorite-type structure for these samples.

3.4 ^{29}Si MAS NMR studies. Table 3 summarizes the ^{29}Si MAS NMR results, and Figure 5 shows a selection of the spectra. Nearly all samples show peaks near –79 and –85 ppm, which are attributable to the Q^1 and Q^2 Si sites, respectively. Q^1 sites can be found on isolated pairs of tetrahedra (i.e. dimers) or on the ends of silicate chains; Q^2 sites are found in the middle of the chains. The absence of Q^0 (monomer) or Q^3 sites (cross-linking) sites, which resonate near –71 and –94 ppm, respectively, is a good confirmation that the silicate species in C–S–H are dimers and short-to-intermediate length chains.

Moreover, the lack of detectable amounts of Q^0 in the samples made from Ca_3SiO_5 is a good indication these samples were nearly fully reacted. The hydroxylated Q^3(OH) (–101 ppm) and Q^4 sites (–110 ppm) observed in sample L5 (Ca/Si = 0.17) can be assigned to hydrous silica, in agreement with the XRD evidence.

In some of the spectra, the Q^2 peak has a shoulder near –83 ppm. This shoulder has been observed by a number of investigators[10,20-24], but its assignment is still unclear. It is generally assumed that the shoulder is produced by a subset of the Q^2 Si, and it is likely to represent those present as bridging tetrahedra. The current results are consistent with this last hypothesis, as the shoulder becomes increasingly prominent as the Ca/Si ratio decreases. This agreement, however, does not rule out the possibility that the shoulder at –83 ppm can be attributed to certain Q^1 sites, an assignment which is suggested by recent studies in Al-containing C–S–H systems[25]. Nevertheless, for the purposes of calculating the mean chain length, it will be assumed that the shoulder is an integral part of the main Q^2 peak near –85 ppm. This choice will not affect the major conclusions of the present work, and at worst, will only overestimate the mean chain length for several samples of low Ca/Si ratios.

Mean silicate chain length. Figure 6 shows mean chain lengths plotted as a function of Ca/Si ratio for samples from the Ca_3SiO_5 and double decomposition groups. In both cases, decreases in Ca/Si ratio lead to increases in mean chain length, a result that has been previously shown in other ^{29}Si MAS NMR studies[10,11]. The important new finding of this study, which forms the basis of our interpretations of the variations in C–S–H at high Ca/Si, is that differences in mean chain length are possible for C–S–H preparations of a given Ca/Si ratio. This is clearly supported by the fact that, for Ca/Si ratios above 1, the mean chain lengths of the samples from the Ca_3SiO_5 group are consistently higher than those from the double decomposition group.

Indirect evidence from ^{29}Si MAS NMR for the presence of Ca–OH in C–S–H. A feature of Figure 6, also noted in another study[10], is that both groups of preparations show appreciable increases in polymerization only when the Ca/Si ratio decreases below 1.2–1.3. Yu et al.[26] noted that the relative

constancy of the mean chain length at Ca/Si ratios above 1.3 could be explained if the predominant cause of variation in Ca/Si ratio was solid solution with $Ca(OH)_2$, which could be accommodated structurally by omission of entire chain segments, thereby creating Ca–OH bonds and jennite-like environments in C–S–H. This would not affect the polymerization of the silicate anions. Yu et al. considered that at lower Ca/Si ratios, the dominant mechanism for increasing the Ca/Si ratio was depolymerization due to substitution of interlayer Ca for bridging tetrahedra and associated Si–OH groups, or possibly at surface sites. In this case, the mean chain length would be expected to increase with decreasing Ca/Si ratio.

The above conclusions suggest an important link between changes in silicate polymerization and solubility. As shown in Figure 2, the points of intersection of curve A with curves C and C" occur near 1.2 and 1.3, respectively. Since the mean silicate chain lengths of the Ca_3SiO_5 and double decomposition groups are relatively constant above these Ca/Si values, it is believed that variations in Ca/Si ratio along curves C and C" result primarily from changes in the content of Ca–OH in C–S–H. Appreciable changes in the content of interlayer Ca, and thus in silicate polymerization, therefore only occur along curve A. These hypotheses are supported by charge balance considerations presented in Section 4.2.

Reversibility of silicate polymerization. A new and important finding from the ^{29}Si MAS NMR investigations is that silicate polymerization in C–S–H is reversible. This conclusion is seen clearly in Figure 6 as there is excellent agreement between the results for decalcified samples (unfilled and dotted points) and recalcified samples (filled and partially filled points). The result thus confirms the view that the Ca cations dictate the configuration of the silicate anions in C–S–H, not the other way around as has often been assumed. In fact, the predominant role of the cation in any silicate structure is a well-established phenomenon; for example, if Mg^{2+} is the sole metal cation, or at least the one that is the more important in determining the silicate structure, configurations based on zweierketten (i.e. silicate anions that repeat every two tetrahedra such as found in pyroxenes, amphiboles, talc, etc.) result.

However, if Ca^{2+} is the determining cation, as is the case in C–S–H, quite different silicate structures are produced, some (but not all) of which are based on dreierketten, e.g. tobermorite, wollastonite, xonolite.

Changes in chemical shift of Q^1 and Q^2 Si sites. As seen in Figure 7 for samples of the Ca_3SiO_5 group, the chemical shifts of the Q^1 and Q^2 Si sites shift to increasingly negative values as the Ca/Si ratio of C–S–H decreases. This trend was also seen in the samples of the double decomposition group, although with slightly more scatter. Other ^{29}Si MAS NMR data[,27,28] on C–S–H preparations from lime and silica show the same trend, too, but it was only explicitly noted by Klur et al[21]. These observations suggest a systematic change with Ca/Si ratio in the local structural environment of the Si sites in C–S–H. While it does not appear possible to uniquely determine the cause of this shift, particularly taking into account the extensive disorder in C–S–H, some broad conclusions can nevertheless be made based on empirical correlations between ^{29}Si chemical shift and various structural parameters (see references 29 and 30, and those within). It does not appear, for instance, that the decrease in chemical shift with decreasing Ca/Si ratio is caused solely by the progressive replacement of Si–O–Ca with Si–O–H, as might be inferred from IR[26] or ^{17}O MAS NMR evidence, or from the results of the current study; based only on the differences in group electronegativity[31] of the OH and OCa groups, the expected result of such a replacement would be an increase in chemical shift, which is not observed. It is more likely, therefore, that the major contribution to the decrease in chemical shift is a decrease in Si–O distance, or increase in Si–O–cation angle[32], or both. These changes could conceivably result from tilting of tetrahedra, stacking disorder, or, as will be argued in the current study, a transition in C–S–H from a jennite-type to a tobermorite-type conformation with decreasing Ca/Si ratio.

3.5 Ca/Si versus pH. Figure 8 shows a plot of pH versus the Ca/Si ratio of the solid as measured in the phase equilibrium determinations. There does not appear to be a significant difference in pH between the solutions in equilibrium with samples of the Ca_3SiO_5 and double decomposition groups. This however is expected, since the Ca concentrations are 1–2 orders of magnitude greater than those of Si at high Ca/Si ratios, and the pH in solution is primarily determined by the need to balance the charge

of the Ca^{2+} and $CaOH^{+}$ ions in solution.

4 Discussion

4.1 Published values of Ca versus Si concentration. Solubility in the $CaO–SiO_2–H_2O$ system at room temperature has been studied for over a century, so the discovery of two new solubility curves, C and C", might raise some justifiable skepticism. A reevaluation of published data for Ca versus Si concentration was therefore undertaken and, to our satisfaction, very good support for the new curves were found in these data, which verified the existence of a new family of solubility curves at high Ca concentrations.

Figure 9 shows the plots the published data from several well-known investigations, most of which were selected for the completeness of their data sets. Some of the points at high Ca concentrations were not plotted in the earlier depiction[15] of the solubility phase diagram either because data sets were considered erratic (such as those of Kalousek[33]), or difficult to obtain since they were plotted rather than tabulated[9,34]; for the latter cases, "new" data points shown in Figure 9 were obtained from image analysis of digitally scanned figures. Not shown because they would obscure most of the other data points are the many data points obtained by Brown et al.[35] from Ca_3SiO_5 and water at 24°C, using water:solid ratios of 0.7–20, and ages of 30 s–4 h. With increasing age in this range, the concentrations moved along or close to curve A from low Ca concentration to supersaturation in $Ca(OH)_2$ at ~30 mM Ca, and then back to saturation at ~21 mM Ca.

As seen in the plot, there is excellent support for curves C and C", and evidence for a similar curve, C'. Ca/Si ratios of the solids equilibrated at, or nearest to, the intersections of these new curves with curve A and the solubility curve of $Ca(OH)_2$ are noted. Relevant details for individual data sets are given below.

Curve C. This is drawn from the data of the present investigation (mature Ca_3SiO_5 paste) and from most of those obtained by Kalousek[33] (lime-silica at 25°C). Two points from the latter study[33], at 4.2 and 5.8 mM Ca, seem inconsistent with the rest since they lie on curve A rather than C. Samples 21, 23,

and 26 in the same study[33] were excluded because they gave points lying substantially above curve B. One data point out of the four obtained by Greenberg and Chang[17] for mature Ca_3SiO_5 paste at 25°C also lies on this curve. C–S–H equilibrated at the intersection of curve C with A occurs at a Ca/Si ratio near 1.2.

Curve C'. This is drawn from the data of Flint and Wells[34] (lime-silica at 30°C). The nearest point to the intersection with A is associated with C–S–H of Ca/Si equal to 1.25.

Curve C". This is drawn from the data of Greenberg and Chang[17] (lime-silica, prepared at 50°C and equilibrated at 25°C), and that of Roller and Ervin[36] (double decomposition, 30°C). The remaining 3 points from Greenberg and Chang[17] for mature Ca_3SiO_5 paste lie on this curve or between it and curve A. C–S–H samples equilibrated at the intersection of curve C" with A have Ca/Si ratios near 1.3.

Curve A. This is drawn from the data of Brown et al.[35] (Ca_3SiO_5, described above), Taylor[9] (double decomposition, 17°C), and Fujii and Kondo[37] (double decomposition, samples prepared at 20°C and equilibrated at 30°C). These last data were taken from the authors' Fig. 2 rather than from the values listed in the table on p. 649 and in Table II of another reference[38], since the latter were based on a thermodynamic fit, which gives misleadingly high Ca/Si ratios for C–S–H. Ca/Si ratios of C–S–H samples equilibrated at the intersection of curve A with the solubility curve for $Ca(OH)_2$ are near 1.5.

Other possible curves. The data of Grutzeck et al.[39] (lime-silica at 25°C) suggest the possibility of a curve higher in Si concentrations than curve C. The curve is not labeled due to the lack of points at high Ca concentrations. The intersection of this curve with A occurs at a Ca/Si ratio near 1.

The cumulative data in Figure 9 establish the existence of a family of well-defined solubility curves at high Ca concentrations. Stable C–S–H phases prepared at room temperature, thus, do not equilibrate solely on curve A as has been widely assumed. The departures from this curve do not appear to be unambiguously related to variables such as temperature or starting materials, although all the data for preparations by double decomposition seem to show a tendency to equilibrate along curves with low Si concentrations such as A or C". The parallel nature of curves C, C', and C" suggest that the differences

in the curves may result from some variable feature of the C–S–H structure. As will be more firmly established in ensuing sections, we propose that curves C, C' and C" arise from the presence in the C–S–H of Ca–OH bonds; the differences in Si concentrations among these curves are shown to be associated with differences in the mean silicate chain length.

Modification of Curve B at high Ca concentration. Comparison of Figures 2 and 9 with the original depiction[15] of curve B shows that B has been modified at high Ca concentrations. This change was suggested mainly by the establishment of curve C since it became clear that the published solubility data for the early hydration of Ca_3SiO_5 clustered near 20 mM Ca should be assigned to curve C rather than to B as originally drawn. Most of the points in question were for Ca_3SiO_5 that had hydrated for more than several hours, by which time it is reasonable to assume that C–S–H, of the kind apparently found on curve C, had formed. Another shortcoming of the original curve B was that it was not well-substantiated in the region supersaturated in $Ca(OH)_2$. A reassessment of the solubility data for the early hydration of Ca_3SiO_5 was thus undertaken; several of the more complete studies[34,40,41] with data at high Ca concentrations are shown as filled points in Figure 9. From these data, a modified extension of curve B at high Ca concentrations has been made.

Modification to the solubility curve of $Ca(OH)_2$. Since C–S–H of the Ca_3SiO_5 group was in true equilibrium with solid $Ca(OH)_2$ near 20.6 mM Ca, it was concluded that the original depiction of the solubility curve for $Ca(OH)_2$, which curved to higher Ca concentrations with increasing Si concentrations, was in error. This conclusion seems to be supported by the fact that the solubility of pure $Ca(OH)_2$ at 22°C is also 20.6 mM Ca (from linear interpolation of data in reference 42). The solubility curve for $Ca(OH)_2$ is thus redrawn as in Figures 2 and 9.

4.2 Hypothesis for the structural variations in C–S–H at high Ca/Si ratios. Figure 9 shows that variations in solubility for stable C–S–H phases occur at Ca/Si ratios above ~ 1. The problem in rationalizing them is thus one of explaining how the C–S–H structure can vary at these compositions. A fundamental premise of the present hypothesis is that a given Ca/Si ratio can arise from more than one

ionic constitution. C–S–H with a Ca/Si ratio of 0.8, for example, can increase its Ca/Si ratio through (1) omission of bridging silicate tetrahedra, (2) increase in interlayer Ca balanced by loss of protons from Si–OH groups, (3) increase in Ca balanced by OH, or (4) various combinations of these effects. Thus, in the range of Ca/Si ratio above ~ 1 with which we are most concerned, a given Ca/Si ratio can theoretically be achieved by a combination of small mean chain length (i.e. many missing bridging tetrahedra) and low Ca–OH content, or by a higher mean chain length (i.e. more bridging tetrahedra) and higher Ca–OH content. The hypothesis put forth here is that curve C represents C–S–H with a relatively high mean chain length and high Ca–OH content, and that curves C', C" and the portion of A at high Ca concentration represent C–S–H of progressively lower mean chain length and lower Ca–OH content.

Support of the hypothesis from mean silicate chain lengths. The ^{29}Si MAS NMR results shown in Figure 6 are consistent with the above hypothesis since mean chain lengths for samples on curve C (Ca_3SiO_5 group) were consistently higher than those of samples on C" (double decomposition group). While the differences are not dramatic, they are likely real, since the changes in mean chain length were reversible.

Further support for the hypothesis can be found in the literature, which appears to confirm that a minimum mean silicate chain length of 2 occurs in C–S–H that equilibrates on curve A at high Ca concentration. In the reaction between Ca_3SiO_5 and water, the concentrations lie on curve B for so long as unreacted Ca_3SiO_5 remains[15], or more probably for as long as it remains in effective contact with the solution. When the Ca_3SiO_5 surface is no longer sufficiently accessible, and especially if the solution is filtered, the concentrations move onto or near curve A[34,35,41]. ^{29}Si MAS NMR studies on Ca_3SiO_5 pastes show that during the induction period, which typically occupies some 4 h, the silicate ions in the hydration product are monomeric and that for the next day or somewhat longer they are predominantly dimeric[43-46], larger species only forming later. The formation of dimer may reasonably be presumed to coincide with the movement onto curve A. In another study[47], ^{29}Si MAS NMR results showed that

preparations made by double decomposition, using a procedure slightly different from that used in the current study, had Ca/Si ratios between approximately 1.5 and 0.8 with corresponding mean chain lengths between 2.2 and 2.8. These values are consistently lower than those of samples on curve C" in the current study. Given this observation and the fact that preparations made by double decomposition seem to equilibrate only along curves A or C", it can be concluded with some confidence that the chain length in C–S–H found on A at high Ca concentration is low, falling to 2 near saturation in $Ca(OH)_2$.

Charge balance calculation for the presence of Ca–OH in C–S–H. With the assumptions described below, it is possible to calculate, as a function of the mean chain length in C–S–H, the Ca/Si ratio above which Ca–OH must be present. This calculation is useful for testing the hypothesis presented above since the interpretation is implicitly based on the idea that Ca–OH groups are introduced into C–S–H at the points of intersection of curves A with C, C', or C" (Figure 9).

In calculating the Ca/Si ratios at these points, a tobermorite-like structure with a variable mean chain length is assumed to equilibrate along curve A. Since a distribution of chain lengths is possible, the mean chain length is not restricted to the ($3n$–1) values expected for a fragmented dreierketten, and it need not be integral. Evidence from IR spectroscopy[26] and ^{29}Si MAS NMR[10] suggests that Si–OH and Ca–OH do not co-exist in C–S–H, the former being present only at low Ca/Si ratios, the latter at high Ca/Si. At Ca/Si ratios of 1.2–1.3 neither is present, which is the situation at the points of intersection between curves A with C, C', or C". If all silicate tetrahedra are present at these points, the formula at the intersection is thus $Ca_6(Si_6O_{18})\cdot nH_2O$. Removal of bridging tetrahedra is equivalent to removal of the elements of SiO_2, leading to a more general formula, $Ca_6(Si_{6-x}O_{18-2x})\cdot nH_2O$, where x need not be integral. The formula is referred to 6 Si sites. The Ca/Si ratio at the intersection is equal to $(l+1)/l$, where l is the mean chain length. Samples with long mean chain lengths will therefore form Ca–OH, and thus depart from curve A, at lower Ca/Si ratios, while those with shorter chain lengths form Ca–OH at higher values.

The results of the calculation shown in Table 4 agree very well with experimental values and evidence

from the literature. At the intersection of curves A and C (Figure 9), for example, the nearest point from the Ca_3SiO_5 group is sample C2, which has a mean chain length of 5.0 and a Ca/Si ratio of 1.22; the calculated Ca/Si ratio for this mean chain length is 1.20. At the intersection of curves A and C", sample F2 of the double decomposition group has a mean chain length of 2.9 and a Ca/Si ratio of 1.28, the calculated value being 1.33. At the intersection of curve A with the solubility curve of $Ca(OH)_2$, the mean chain length, as argued earlier, is likely near 2, while the Ca/Si ratio, as suggested by the data in Figure 9, is near 1.5. According to the calculations, these values imply that C–S–H equilibrating exclusively along curve A can maintain a purely tobermorite-type structure (i.e. one with no Ca–OH) up to saturation in $Ca(OH)_2$.

Curves A, C", C' and C thus represent C–S–H with progressively increasing degrees of silicate polymerization, which, as shown by charge balance calculations, necessitates the presence in them of Ca–OH.

4.3 Ca–OH content in C–S–H. *Charge balance*. The agreement with the calculations shown above suggests that Ca^{2+} ions rather than protons in Si–OH groups preferentially balance the silicate anions in C–S–H. Since Ca not balanced by silicate anions must form parts of Ca–OH groups, it is possible to calculate, as a function of the mean chain length and Ca/Si ratio, the Ca–OH content in C–S–H. Values, which are reported as the fraction of Ca in C–S–H balanced by OH, are represented in Figure 10 as open symbols for the Ca_3SiO_5 and double decomposition groups. Samples of the Ca_3SiO_5 group have a considerably higher Ca–OH content than those of the double decomposition group; at saturation in $Ca(OH)_2$, the fraction of Ca balanced by OH is approximately 25% in C–S–H produced from Ca_3SiO_5, and about 6% in that produced by double decomposition. These values are consistent with the idea that Ca–OH contents for a given Ca/Si ratio are highest on curve C and progressively lower on C', C", and A (Figure 9).

The solid line in Figure 10 is a best-fit curve for the computed values of the Ca_3SiO_5 group; the dashed, parallel line is a presumed relationship for the double decomposition group. The trends show

that Ca–OH contents decrease with Ca/Si ratio and become zero for the Ca_3SiO_5 and double decomposition groups near values of 1.2 and 1.3, respectively. These values are consistent with those found at the intersections of curves A with C and C".

Inelastic neutron scattering. The Ca–OH content in 8-month aged C–S–H produced from Ca_3SiO_5 has recently been quantified[48] by inelastic neutron scattering (INS) spectroscopy. This was done by determining the contribution from C–S–H to the intensity of the energy band at 41 meV, which originates from lattice modes involving the translational oscillations of OH groups attached to Ca[49]. Results, plotted as solid symbols in Figure 10, agree well with the computed values, particularly at high Ca/Si ratios. The slightly higher values measured by INS at Ca/Si ~ 1.1 may suggest the coexistence of Si–OH and Ca–OH at these compositions; however, it is also likely that the higher than expected value reflects the difficulty in measuring the low intensity of the broad band at 41 meV.

Resemblance of C–S–H to jennite. Based on the new constitutional formula for jennite[3], $Ca_9(Si_6O_{18})(OH)_6{\bullet}8H_2O$, the percentage of Ca in jennite balanced by OH is 33%. The value of 25% computed for C–S–H from Ca_3SiO_5 at saturation in $Ca(OH)_2$ is significantly closer to this value than that of 1.4-nm tobermorite, which is theoretically zero. The closer correspondence to the value of jennite supports Taylor's hypothesis[13] that, at late times, the local structure of C–S–H from Ca_3SiO_5 has a closer resemblance to a jennite-type structure than a tobermorite-type structure. This conclusion assumes that Ca–OH bonds occur in the main Ca–O sheet of C–S–H, arranged in a way similar to that in jennite. This assumption is reasonable when the Ca–OH content is high, as on curve C, but may not be when it is low, as on C" (Figure 9). In the latter case, a largely tobermorite-like structure may be maintained in solid solution with Ca–OH that has formed from random substitution of OH for silicate anions. This has been the general conclusion for studies on preparations of C–S–H made by lime and silica in suspension, or by double decomposition.

It should be mentioned that the Ca incorporated into C–S–H along curve C, C', or C" may not be entirely in the form of Ca–OH bonds. A minor portion of the Ca may instead substitute for bridging

tetrahedra as suggested by the decrease in mean chain length of samples of the Ca_3SiO_5 group from a value of 5 at the intersection of curves A and C, to 2.8 at the saturation in $Ca(OH)_2$. It is estimated that, along curve C, the ratio of Ca incorporated as Ca–OH to that substituting for bridging tetrahedra is roughly 3:1. It may be revealing that the mean chain length of C–S–H from Ca_3SiO_5 is nearly 5 after 26 years of aging[44]; this could indicate that, with time, all of the Ca incorporated along curve C at bridging tetrahedral sites slowly migrate to Ca–OH sites, thereby forming a purely jennite-type structure.

4.4 Variations in Ca/Si ratio of C–S–H at saturation in $Ca(OH)_2$. A long-standing conundrum in the $CaO–SiO_2–H_2O$ system is the disconcerting variability in the published values of Ca/Si ratios of C–S–H in equilibrium with solid $Ca(OH)_2$ (Table 5). Steinour[14] cites values ranging from 1.2 to ~2, and Table 5 gives a selection of these, with some obtained more recently. Except for preparations made by double decomposition, for which all the data indicate a Ca/Si ratio of 1.4–1.5, there is no apparent relation to the method of preparation, and no adequate explanation has been offered. In the context of the present findings, however, it appears that the variations may be related to differences in the C–S–H structure.

Arguments presented in earlier sections indicate that Ca/Si ratios near 1.5 at saturation in $Ca(OH)_2$ arise from structures that are mainly or wholly based on 1.4-nm tobermorite. This conclusion is strongly supported by the charge balance considerations presented in Section 4.2. Ca/Si ratios greater than 1.5 at $Ca(OH)_2$ saturation appear possible only when equilibration occurs on curve C, C', or C'', that is, when Ca–OH is present. Since higher Ca–OH contents should, in principle, allow for higher Ca/Si ratios, the trends in Ca/Si ratio at saturation in $Ca(OH)_2$ should follow those in Ca–OH content, that is, highest values on curve C and progressively lowers values on C', C'', and A. Although there is scatter, the data in Table 5 suggests that this is the most probable trend. The variations in Ca/Si ratio in C–S–H at saturation in $Ca(OH)_2$ are thus likely caused by differences in Ca–OH contents.

This result reinforces the conclusion that the family of solubility curves at high Ca concentration represent a spectrum of C–S–H structures, ranging from a purely tobermorite-like structure on curve A

to a jennite-like structure on C.

5 Conclusions

New phase equilibrium results and a reassessment of published data demonstrate the existence in the $CaO–SiO_2–H_2O$ system at room temperature of a new family of solubility curves: A, C", C', and C (Figure 9). ^{29}Si MAS NMR studies and charge balance calculations illustrate that these variations in solubility reflect systematic variations in Ca/Si ratio, mean silicate chain length, and Ca–OH content in C–S–H. These trends, summarized below, lead to more explicit relationships between C–S–H and 1.4-nm tobermorite and jennite, as well as to a more comprehensive understanding of the nanostructure of C–S–H.

(i) C–S–H preparations with solubilities following exclusively curve A up to saturation in $Ca(OH)_2$ do not contain Ca–OH, and are thus of purely tobermorite-type. At saturation in $Ca(OH)_2$, these preparations have a Ca/Si ratio of 1.5 and a mean chain length of 2.

(ii) C–S–H preparations of a given Ca/Si ratio can differ in degree of silicate polymerization. For Ca/Si ratios above 1.2, those of the highest observed mean chain lengths equilibrate on curve C. With decreasing mean chain length, C–S–H equilibrates on curves C', C", and finally, A.

(iii) Under the assumption that Ca–OH and Si–OH groups do not coexist, the Ca/Si ratio above which Ca–OH must be present in C–S–H can be calculated from the mean silicate chain length. These values correspond to those present at the points of intersection of curves A with C", C', and C, indicating the presence of Ca–OH on C", C', and C. At a given Ca/Si ratio, the content of Ca–OH progressively increases for C–S–H equilibrated on A, C", C', and C.

(iv) Although there is scatter in the data, the highest Ca/Si ratios at saturation in $Ca(OH)_2$ tend to be given by preparations equilibrating on curve C and progressively lower ratios by those equilibrating on C', C", and A. The higher values are believed to result from higher concentrations of Ca–OH. These tendencies appear to explain some of the broad variations in the Ca/Si ratio at $Ca(OH)_2$ saturation found in the literature.

(v) Assuming that high contents of Ca–OH are accommodated through a jennite-like configuration, curves A, C'', C', and C represent a spectrum of C–S–H configurations at room temperature that range from a purely tobermorite-based structure on curve A to a jennite-like structure on C.

Acknowledgment. This work was supported by the National Science Foundation under Grant No. CMS-0070922/001.

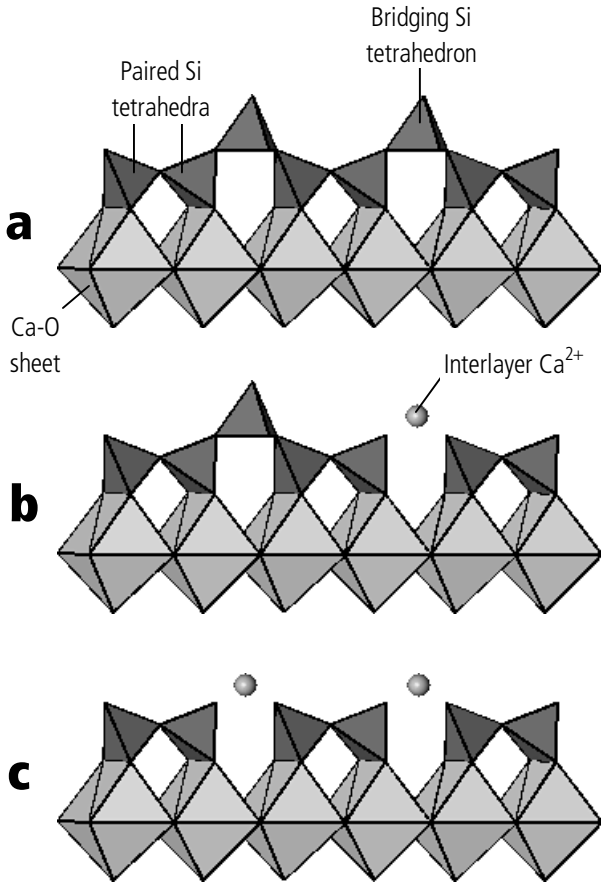

Figure 1. In 1.4-nm tobermorite (a), infinite dreierketten are bonded to rows of sevenfold-coordinated Ca–O polyhedra. One of several mechanisms by which the Ca/Si ratio can increase is the substitution of Ca^{2+} for bridging tetrahedra, thereby fragmenting the silicate chains as illustrated in (b) and (c), the latter showing a minimum silicate chain length of 2. The position of the interlayer Ca^{2+} is merely speculative and likely influenced by water molecules, which are not shown.

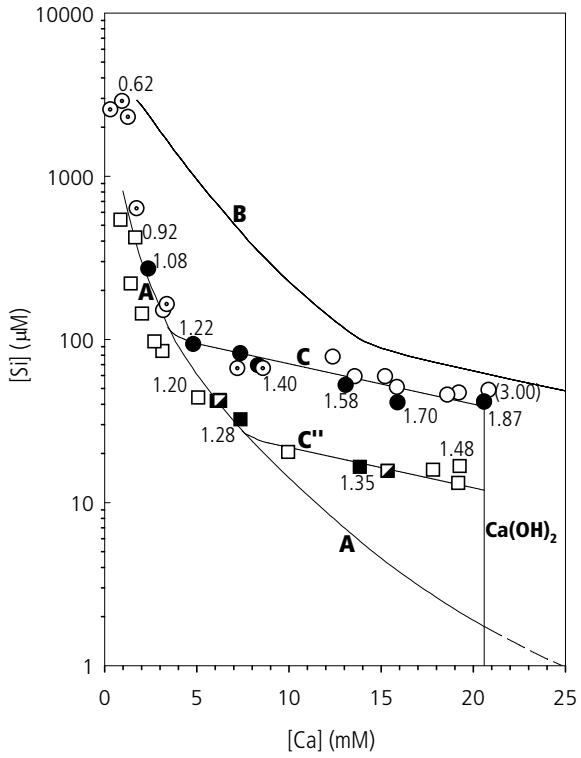

Figure 2. Solubility results for samples derived from Ca_3SiO_5 (○, Series A; ⊙, Series B; ●, Series C) and from double decomposition (□, Series D; ◪, Series E; ■, Series F). Unfilled and dotted points approach equilibrium by decalcification, filled and partially filled points by recalcification. Ca/Si ratios of several solids are noted; the value enclosed in parenthesis denotes a sample containing C–S–H and $Ca(OH)_2$.

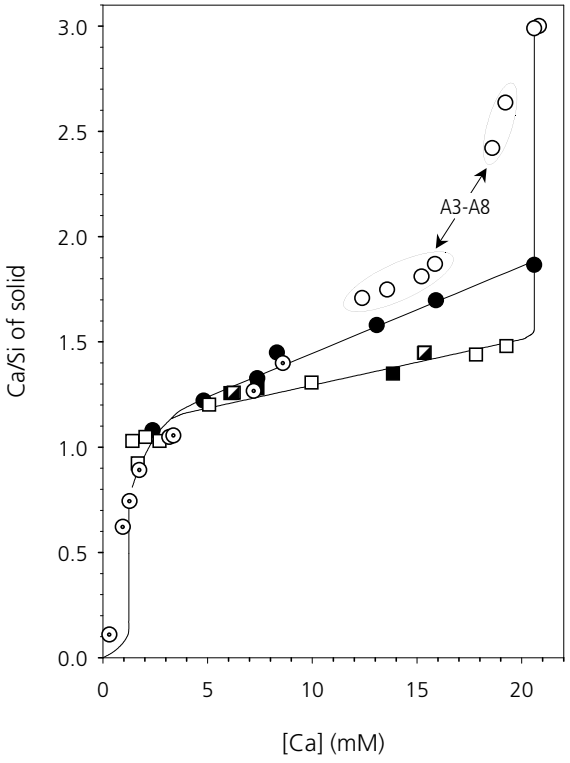

Figure 3. Ca concentration in aqueous solution versus Ca/Si ratios of the solid for samples of the Ca_3SiO_5 (○, Series A; ⊙, Series B; ●, Series C) and double decomposition (□, Series D; ◪, Series E; ■, Series F) groups. Unfilled and dotted points represent decalcified solids, filled and partially filled points recalcified solids. Samples A3–A8 noted on the graph are not believed to be in true equilibrium.

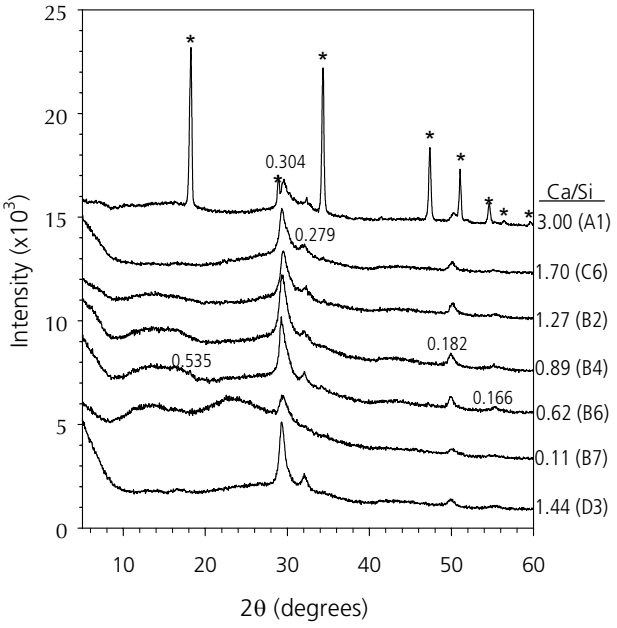

Figure 4. XRD powder scans of selected samples from the Ca_3SiO_5 (samples A1, C6, B2, B4, B6, B7) and double decomposition (sample D3) groups. C–S–H *d*-spacings are noted above their respective peaks in units of nm; peaks associated with $Ca(OH)_2$ are marked with asterisks.

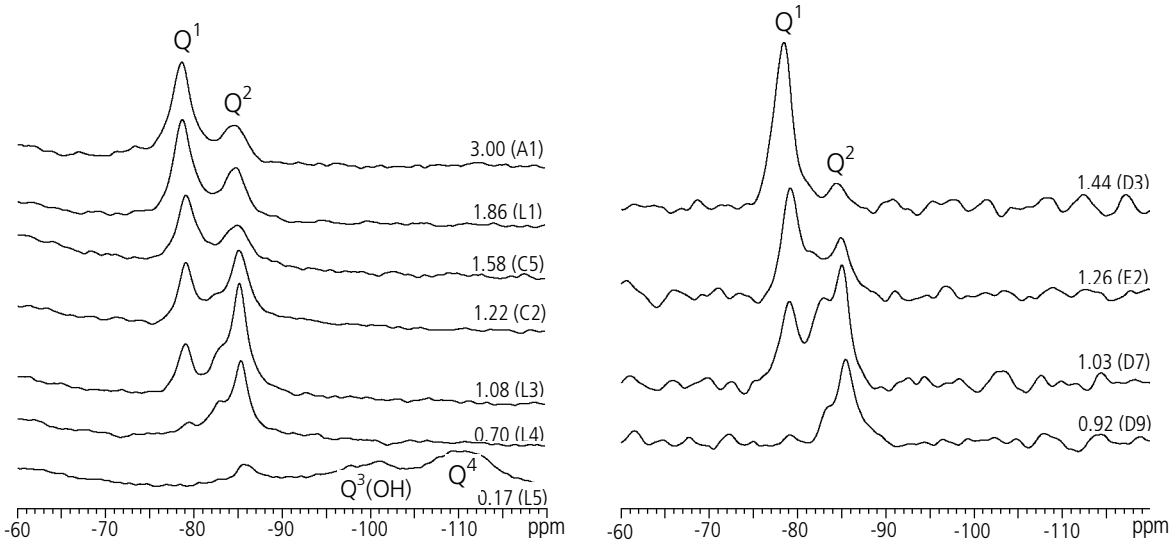

Figure 5. ^{29}Si MAS NMR results for samples from the Ca_3SiO_5 (left) and double decomposition (right) groups. Ca/Si ratios of the solids are noted with sample numbers in parenthesis.

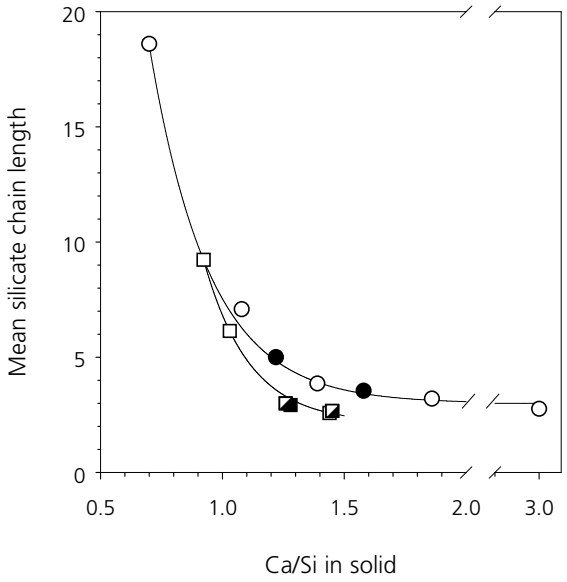

Figure 6. Mean chain lengths calculated from ^{29}Si MAS NMR data for the Ca_3SiO_5 (○, Series L; ●, Series C) and double decomposition (□, Series D; ◪, Series E; ■, Series F) groups. Unfilled points represent decalcified solids, filled and partially filled points recalcified solids.

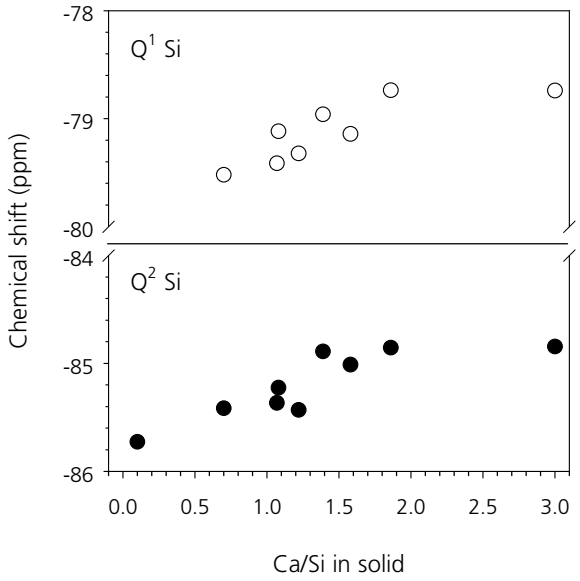

Figure 7. Changes in chemical shift of the Q^1 (○) and Q^2 (●) Si sites as a function of Ca/Si ratio in C–S–H of the Ca_3SiO_5 group.

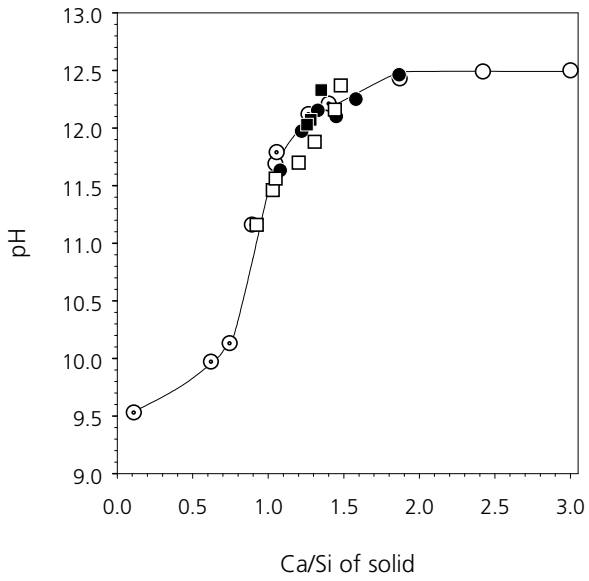

Figure 8. pH values of the aqueous solutions in equilibrium with samples from the Ca_3SiO_5 (○, Series A; ⊙, Series B; ●, Series C) and double decomposition (□, Series D; ■, Series F) groups.

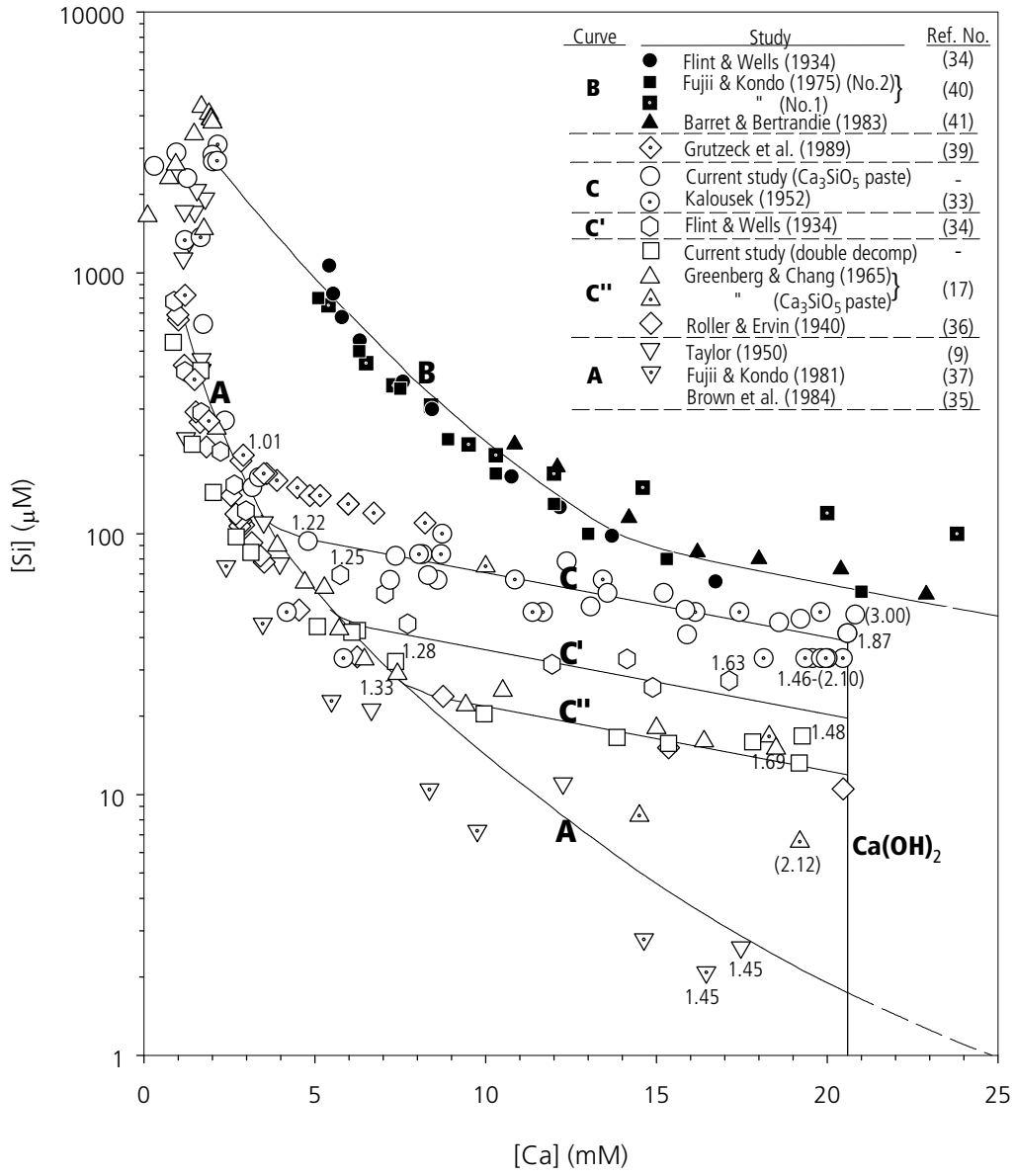

Figure 9. Published solubility data plotted as Ca versus Si concentration in aqueous solution. Unfilled points refer to equilibria for stable C–S–H phases; filled points refer to metastable equilibria occurring during the early hydration of Ca_3SiO_5. Ca/Si ratios of selected solids are noted, and those in parenthesis denote samples containing C–S–H and $Ca(OH)_2$.

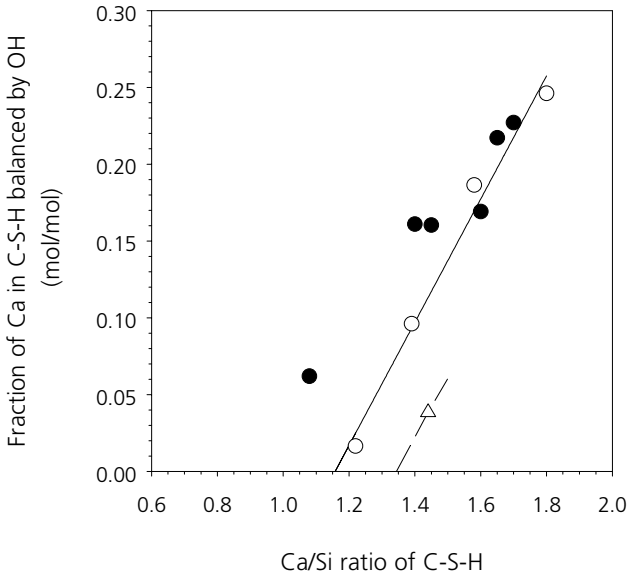

Figure 10. Fraction of Ca in C–S–H balanced by OH. Open symbols are computed from charge balance calculations for the Ca_3SiO_5 (○) and double decomposition (△) groups. The solid line is a best-fit curve for the computed values of the Ca_3SiO_5 group; the dashed, parallel line is a presumed relationship for the double decomposition group. Solid symbols (●) are values based on inelastic neutron scattering data[48] on Ca_3SiO_5 pastes.

Table 1. Preparation of samples for phase equilibrium determinations.

Precursor	Series	Procedure
Ca_3SiO_5 paste	A[a]	Pastes, in their saturated state, were lightly crushed, then equilibrated in H_2O or $Ca(OH)_2$ solutions of various concentrations.
	B[a]	Pastes were leached in NH_4NO_3 solutions to Ca/Si ratios between 0.1 and 2.0, rinsed, crushed, and then equilibrated in H_2O.
	C[b]	Pastes were leached in NH_4NO_3 solution to Ca/Si = 1.09, rinsed, crushed, and then equilibrated in $Ca(OH)_2$ solutions of various concentrations.
C-S-H precipitated from $Ca(NO_3)_2$ + Na_2SiO_3	D[a]	C–S–H was equilibrated in H_2O or $Ca(OH)_2$ solutions of various concentrations.
	E[b]	C–S–H was leached in NH_4NO_3 solution to Ca/Si = 0.55, rinsed, and then equilibrated in $Ca(OH)_2$ solutions of various concentrations.
	F[b]	C–S–H was leached in H_2O by placing ~ 50 g of sample in 500 mL of H_2O. The mixture was repeatedly decanted and replaced with fresh H_2O for a total period of 12 days until the Ca/Si ratio reached 1.05. The solid was then equilibrated in $Ca(OH)_2$ solutions of various concentrations.

[a] The series approaches equilibrium through the decalcification of a high Ca/Si solid.

[b] The series approaches equilibrium by the recalcification of a low Ca/Si solid.

Table 2. Summary of the phase equilibrium results.

Precursor and *treatment*	Sample	$Ca/Si_{initial}$	[Ca] (mM)	[Si] (μM)	pH	Ca/Si_{final}	Phases present[a]
Ca_3SiO_5	A1	3.00	20.83	48.9	–[b]	3.00	C–S–H, $Ca(OH)_2$
	A2	3.00	20.59	41.5	–	2.99	–
	A3	3.00	19.22	47.1	–	2.64	–
	A4	3.00	18.59	45.7	12.49	2.42	C–S–H, $Ca(OH)_2$
Equilibrated in H_2O or $Ca(OH)_2$ solution	A5	3.00	15.86	51.1	12.43	1.87	C–S–H, $Ca(OH)_2$
	A6	3.00	15.22	59.3	–	1.81	–
	A7	3.00	13.57	59.3	–	1.75	–
	A8	3.00	12.38	78.2	–	1.71	C–S–H, $Ca(OH)_2$
	A9	3.00	3.17	150.7	11.69	1.05	–
	B1	2.04	8.59	66.4	12.21	1.40	–
Leached in NH_4NO_3 solution, then equilibrated in H_2O	B2	1.56	7.20	66.4	12.12	1.27	C–S–H
	B3	1.21	3.37	164.3	11.79	1.06	–
	B4	0.98	1.73	635.3	11.16	0.89	C–S–H
	B5	0.74	1.27	2303.6	10.13	0.74	–
	B6	0.56	0.95	2890.7	9.97	0.62	C–S–H
	B7	0.11	0.30	2565.7	9.53	0.11	C–S–H, SiO_2 gel
	C1	1.09	2.37	271.1	11.63	1.08	–
Leached in NH_4NO_3 solution, then equilibrated in $Ca(OH)_2$ solution	C2	1.09	4.81	93.6	11.97	1.22	–
	C3	1.09	7.36	82.1	12.15	1.33	C–S–H
	C4	1.09	8.31	69.3	12.10	1.45	–
	C5	1.09	13.08	52.5	12.25	1.58	–
	C6	1.09	15.90	41.1	–	1.70	C–S–H
	C7	1.09	20.59	41.5	12.46	1.87	C–S–H
	L1	3.00	–	–	–	1.86	–
Leached in NH_4NO_3 solution	L2	3.00	–	–	–	1.39	–
	L3	3.00	–	–	–	1.08	–
	L4	3.00	–	–	–	0.70	–
	L5	3.00	–	–	–	0.17	–
$Ca(NO_3)_2 + Na_2SiO_3$	D1	1.40	19.27	16.8	12.37	1.48	C–S–H
	D2	1.40	19.18	13.2	–	–	–
	D3	1.40	17.82	15.9	12.16	1.44	–
	D4	1.40	9.96	20.4	11.88	1.31	–
Equilibrated in H_2O or $Ca(OH)_2$ solution	D5	1.40	5.08	44.1	11.70	1.20	–
	D6	1.40	3.13	84.9	–	–	–
	D7	1.40	2.70	97.3	11.46	1.03	–
	D8	1.40	2.03	144.0	11.56	1.05	–
	D9	1.40	1.66	421.6	11.16	0.92	C–S–H
	D10	1.40	1.41	220.4	–	1.03	–
	D11	1.40	0.86	541.4	–	–	–
Leached in NH_4NO_3 solution, then equilibrated in $Ca(OH)_2$ solution	E1	0.55	15.36	15.7	–	1.45	–
	E2	0.55	6.25	42.5	–	1.26	–
Leached in HO, then equilibrated in $Ca(OH)_2$ solution	F1	1.05	13.85	16.6	12.33	1.35	–
	F2	1.05	7.37	32.4	12.07	1.28	C–S–H
	F3	1.05	6.09	41.9	12.03	1.26	–

[a] Phase identification was determined by XRD.

[b] Dashes indicate a property that was not determined.

Table 3. ^{29}Si MAS NMR results for C–S–H derived from Ca_3SiO_5 and from double decomposition of $Na_2SiO_3 + Ca(NO_3)_2$.

Precursor	Sample	Ca/Si	Mean silicate chain length[a]	Q^1 (ppm)	Q^2 (ppm)	Q^2 shoulder (ppm)	Q^3(OH) (ppm)	Q^4 (ppm)
Ca_3SiO_5	A1	3.00	2.8	-78.7	-84.8			
	L1	1.86	3.2	-78.7	-84.9			
	C5	1.58	3.5	-79.1	-85.0			
	C2	1.22	5.0	-79.3	-85.4			
	L2	1.39	3.9	-79.0	-84.9			
	L3	1.08	7.1	-79.1	-85.2	-83.1		
	L4	0.70	18.6	-79.5	-85.4	-83.0		
	L5	0.10	high		-85.7		-101.3	-109.6
Na_2SiO_3 +	D3	1.44	2.6	-78.5	-84.3			
$Ca(NO_3)_2$	F2	1.28	2.9	-78.7	-84.7	-82.2		
	E2	1.26	3.0	-79.4	-85.2			
	D7	1.03	6.1	-79.1	-85.1	-82.8		
	D9	0.92	9.2	-78.7	-85.0	-82.9		

[a] Calculated from relative intensity of Q^2 and Q^1 Si peaks.

Table 4. Charge balance calculations for the Ca/Si ratio above which Ca–OH must be present in C–S–H.

Mean silicate chain length	Formula per 6 Si sites[a]	Ca/Si ratio above which Ca–OH must be present[b]
2	$Ca_6Si_4O_{14}$	1.50
3	$Ca_6Si_{4.5}O_{15}$	1.33
4	$Ca_6Si_{4.8}O_{15.6}$	1.25
5	$Ca_6Si_5O_{16}$	1.20
∞	$Ca_6Si_6O_{18}$	1.00

[a] Molecular water is omitted.

[b] The calculation assumes a tobermorite-like C–S–H of variable mean chain length is present along curve A with the restriction that Si–OH and Ca–OH do not coexist.

Table 5. Published values of the Ca/Si ratio in C–S–H determined at saturation in $Ca(OH)_2$.

Method of preparation	Author(s)	Ref. No.	Starting materials	Ca/Si at $Ca(OH)_2$ saturation	Solubility curve at high Ca concentration
Double decomposition	Bessey	(50)	$Na_2SiO_3 + Ca(NO_3)_2$	1.5	-
	Taylor	(9)	$Na_2SiO_3 + Ca(NO_3)_2$	1.5	A
	Fujii & Kondo	(37)	$Na_2SiO_3 + Ca(NO_3)_2$	1.5	Below A
	Current study	-	$Na_2SiO_3 + Ca(NO_3)_2$	1.5	C"
	Roller & Ervin	(36)	$Na_2SiO_3 + Ca(OH)_2$	1.4	C"
Lime and silica suspensions	Baylis	(51)	$CaO + SiO_2$	1.7	-
	van der Burgh	(52)	$CaO + SiO_2$	1.4	-
	Shaw & MacIntire	(53)	$CaO + SiO_2$	1.4	-
	Le Chatelier	(54)	$Ca(OH)_2 + SiO_2$	1.7	-
	Flint & Wells	(34)	$Ca(OH)_2 + SiO_2$	1.7	C'
	Kalousek	(33)	$Ca(OH)_2 + SiO_2$	1.3 or 1.7[a]	C
	Cong & Kirkpatrick	(10)	$Ca(OH)_2 + SiO_2$	1.6	-
	Greenberg & Chang	(17)	$Ca(OH)_2 + SiO_2$	1.7	C"
Anhydrous calcium silicates	Kuhl & Mann	(55)	CaO/SiO_2 melt	1.5	-
	Cong & Kirkpatrick	(10)	Reactive Ca_2SiO_4	1.5	-
	Thorvaldson & Vigfusson	(56)	Ca_2SiO_4, Ca_3SiO_5	1.4	-
	Nonat & Lecoq	(57)	Ca_3SiO_5	1.4	-
	Cirilli	(58)	Ca_3SiO_5	1.4	-
	Taylor	(9)	Ca_3SiO_5 (2 points)	1.6	-
	Greenberg & Chang	(17)	Mature Ca_3SiO_5 paste	1.8	A,C",C
	Current study	-	Mature Ca_3SiO_5 paste	1.8	C

[a] Evidence is presented for both the low and high values.

References

(1) Taylor, H. F. W. *Cement Chemistry*, 2nd ed.; Thomas Telford: London, 1997.

(2) Merlino, S.; Bonaccorsi, E.; Kampf, A. R. In *Applied Mineralogy*; Rammlmair, D.; Mederer, J.; Oberthür, T.; Heimann, R. B.; Pentinghaus, H.; Eds.; Balkema: Rotterdam, 2000; pp 859-861.

(3) Bonaccorsi, E.; Merlino, S.; Taylor, H. F. W. in preparation.

(4) Taylor, H. F. W.; Howison, J. W. *Clay Minerals Bull.* **1956**, *3*, 98-110.

(5) Komarneni, S.; Roy, D. M. *Science* **1983**, *221*, 647-648.

(6) Matsuyama, H.; Young, J. F. *Chem. Mater.* **1999**, *11*, 16-19.

(7) Alexandre, M.; Dubois, P. *Mater. Sci. Eng. R-Rep.* **2000**, *28*, 1-63.

(8) Taylor, H. F. W. In *Proc. 5th Int. Symp. Chem. Cem.*; Cement Association of Japan: Tokyo, Japan, 1968; pp 1-26.

(9) Taylor, H. F. W. *J. Chem. Soc.* **1950**, 3682-3690.

(10) Cong, X.; Kirkpatrick, R. J. *Advn. Cem. Based. Mat.* **1996**, *3*, 144-156.

(11) Matsuyama, H.; Young, J. F. *Adv. Cem. Res.* **2000**, *12*, 29-33.

(12) Gard, J. A.; Taylor, H. F. W. *Cem. Concr. Res.* **1976**, *6*, 667-678.

(13) Taylor, H. F. W. *J. Am. Ceram. Soc.* **1986**, *69*, 464-467.

(14) Steinour, H. H. *Chem. Rev.* **1947**, *40*, 391-460.

(15) Jennings, H. M. *J. Am. Ceram. Soc.* **1986**, *69*, 614-618.

(16) Barret, P.; Bertrandie, D. *J. Am. Ceram. Soc.* **1988**, *71*, C113-C115.

(17) Greenberg, S. A.; Chang, T. N. *J. Phys. Chem.* **1965**, *69*, 182-188.

(18) Copeland, L. E.; Hayes, J. C. *ASTM Bull.* **1953**, *194*, 70-74.

(19) Farinas, J. C.; Ortega, P. *Analusis* **1992**, *20*, 221-228.

(20) Brough, A. R.; Dobson, C. M.; Richardson, I. G.; Groves, G. W. *J. Am. Ceram. Soc.* **1994**, *77*, 593-596.

(21) Klur, I.; Pollet, B.; Virlet, J.; Nonat, A. In *Nuclear Magnetic Resonance Spectroscopy of Cement-Based Materials*; Colombet, P.; Grimmer, A.-R.; Zanni, H.; Sozzani, P.; Eds.; Springer: Berlin, 1998; pp 119-141.

(22) Richardson, I. G. *Cem. Concr. Res.* **1999**, *29*, 1131-1147.

(23) Komarneni, S.; Roy, R.; Roy, D. M.; Fyfe, C. A.; Kennedy, G. J.; Bothner-By, A. A.; Dadok, J.; Chesnick, A. S. *J. Mater. Sci.* **1985**, *20*, 4209-4214.

(24) Sun, G.; Brough, A. R.; Young, J. F. *J. Am. Ceram. Soc.* **1999**, *82*, 3225-3230.

(25) Brough, A. R.; Richardson, I. G. personal communication with H.F.W. Taylor.

(26) Yu, P.; Kirkpatrick, R. J.; Poe, B.; McMillan, P. F.; Cong, X. *J. Am. Ceram. Soc.* **1999**, *82*, 742-748.

(27) Popova, A.; Geoffroy, G.; Renou-Gonnard, M.-F.; Faucon, P.; Gartner, E. *J. Am. Ceram. Soc.* **2000**, *83*, 2556-2560.

(28) Viallis, H.; Faucon, P.; Petit, J. C.; Nonat, A. *J. Phys. Chem. B.* **1999**, *103*, 5212-5219.

(29) Englehardt, G.; Michel, D., *High-Resolution Solid-State NMR of Silicates and Zeolites*; New York: John Wiley & Sons, 1987; Chapter 4.

(30) Englehardt, G.; Koller, H. In *NMR Basic Principles and Progress*; Diehl, P.; Fluck, E.; Gunther, H.; Kosfeld, R.; Seelig, J.; Eds.; Springer-Verlag: Berlin, 1994; pp 3-29.

(31) Janes, N.; Oldfield, E. *J. Am. Chem. Soc* **1985**, *107*, 6769-6775.

(32) Sherriff, B. L.; Grundy, H. D. *Nature* **1988**, *332*, 819-822.

(33) Kalousek, G. L. In *Proc. 3rd Int. Symp. Chem. Cem.*; Cement and Concrete Association: London, 1952; pp 296-311.

(34) Flint, E. P.; Wells, L. S. *J. Res. Natl. Bur. Stds.* **1934**, *12*, 751-783.

(35) Brown, P. W.; Franz, E.; Frohnsdorff, G.; Taylor, H. F. W. *Cem. Concr. Res.* **1984**, *14*, 257-262.

(36) Roller, P. S.; Ervin, G. *J. Am. Chem. Soc.* **1940**, *62*, 461-471.

(37) Fujii, K.; Kondo, W. *J. Chem. Soc. Dalt. Trans.* **1981**, *2*, 645-651.

(38) Fujii, K.; Kondo, W. *J. Am. Ceram. Soc.* **1983**, *66*, C-220-C221.

(39) Grutzeck, M.; Benesi, A.; Fanning, B. *J. Am. Ceram. Soc.* **1989**, *72*, 665-668.

(40) Fujii, K.; Kondo, R. *Nippon Seram. Kyo. Gak.* **1975**, *83*, 214-226.

(41) Barret, P.; Bertrandie, D. *J. Chim. Phys.* **1983**, *83*, 765-775.

(42) Bassett, H. *J. Chem. Soc.* **1934**, 1270-1275.

(43) Lippmaa, E.; Magi, M.; Tarmak, M.; Wieker, W.; Grimmer, A. R. *Cem. Concr. Res.* **1982**, 597-602.

(44) Rodger, S. A.; Groves, G. W.; Clayden, N. J.; Dobson, C. M.. In *Proc. Mat. Res. Soc Symp.*; Struble, L. J.; Brown, P. W.; Eds.; Materials Research Society: Pittsburgh, 1987; pp 13-20.

(45) Rodger, S. A.; Groves, G. W.; Clayden, N. J.; Dobson, C. M. *J. Am. Ceram. Soc.* **1988**, *71*, 91-

96.

(46) Brough, A. R.; Dobson, C. M.; Richardson, I. G.; Groves, G. W. *J. Mater. Sci.* **1994**, *29*, 3926-3940.

(47) Cong, X.; Kirkpatrick, R. J. *Cem. Concr. Res.* **1993**, *23*, 1065-1077.

(48) Thomas, J. J.; Neumann, D. A.; Chen, J. J.; Jennings, H. M. in preparation.

(49) Baddour-Hadjean, R.; Fillaux, F.; Flouquet, N.; Belushkin, S.; Natkaniec, I.; Desgranges, L.; Grebille, D. *Chem. Phys.* **1995**, *197*, 81-90.

(50) Bessey, G. E. In *Proc. Symp. Chem. Cem.*; Ingeniörsvetenskapsakademien: Stockholm, 1938; pp 179-215.

(51) Baylis, J. *J. Phys. Chem.* **1928**, *32*, 1236-1262.

(52) van der Burgh, A. J. P. *Chem. Weekblad* **1932**, *29*, 616-618.

(53) Shaw, W. M.; MacIntire, W. H. *Soil Sci.* **1930**, *29*, 429-456.

(54) Le Chatelier, H. *Ann. Mines* **1887**, *11*(8), 345-465.

(55) Kühl, H.; Mann, A. *Tonind.-Ztg* **1934**, *58*, 862-865,896-897,918-919,930-932,944-945,955-957,990-991,1003,1014-1016.

(56) Thorvaldson, T.; Vigfusson, V. A. *Trans. R. Soc. Can.* **1928**, *3*(22(III)), 423-431.

(57) Nonat, A.; Lecoq., X., In *Nuclear Magnetic Resonance Spectroscopy of Cement-Based Materials*; Colombet, P.; Grimmer, A.-R.; Zanni, H.; Sozzani, P.; Eds.; Springer: Berlin, 1998; pp 197-207.

(58) Cirilli, V. *Ricerca Sci.* **1939**, *10*, 459-61.